Jurnal Teknologi

Full Paper

ENHANCING RARE EARTH ELEMENTS STABILITY IN ION ADSORPTION CLAYS DURING ION-EXCHANGE LEACHING WITH SALT SOLUTIONS: A THERMODYNAMIC APPROACH THROUGH POURBAIX DIAGRAMS

Nurul Aniyyah Mohamad Sobri[a,c], Noorlisa Harun[a*], Mohd Yusri Mohd Yunus[b]

[a]Faculty of Chemical and Process Engineering Technology, UMPSA, Kuantan, Pahang, Malaysia
[b]Centre for Sustainability of Ecosystem & Earth Resources, UMPSA, Kuantan, Pahang, Malaysia
[c]Faculty of Engineering Technology, UC TATI, Kemaman, Terengganu, Malaysia

Article history
Received
1 August 2024
Received in revised form
16 April 2025
Accepted
3 May 2025
Published Online
24 December 2025

*Corresponding author
noorlisa@umpsa.edu.my

Graphical abstract

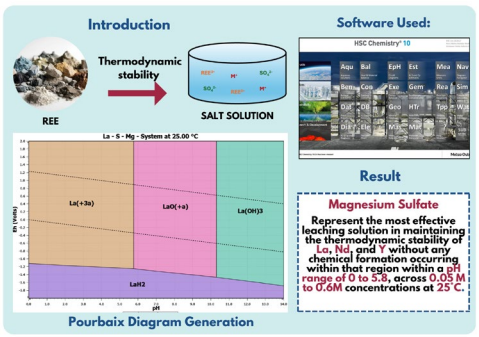

Abstract

Rare Earth Elements (REEs) are typically extracted from ion adsorption clays using the ion-exchange leaching method, which involves a salt solution as the leaching solution. To maximize REE leaching efficiencies, it is crucial to maintain the thermodynamic stability of REEs in the salt solution during the extraction process. Therefore, a thermodynamic approach through the Pourbaix diagram was conducted by using HSC Chemistry 10.0 software. In this study, the three most significant REE concentrations in ion adsorption clay- lanthanum (La), neodymium (Nd), and yttrium (Y)- were tested using different sulfate solutions (ammonium sulfate, magnesium sulfate, and aluminum sulfate) across concentrations ranging from 0.05 to 0.6 M and temperatures from 25 to 80 °C. The Pourbaix diagrams analysis demonstrated that magnesium sulfate solution was the most effective leaching solution, providing the maximum thermodynamic stability for La, Nd, and Y within a pH range of 0 to 5.8, across all tested concentrations, without any chemical formation occurring within that region. Additionally, the stability of La, Nd, and Y was found to decrease as the leaching temperature increased. Since 25°C proved to be the optimal temperature in this study, it suggests that ion-exchange leaching can be efficiently performed at ambient temperature, eliminating the need for external heating during the extraction process. In conclusion, using magnesium sulfate as a leaching solution at ambient leaching temperature enhances the thermodynamic stability of REEs in ion adsorption clay during ion-exchange leaching, leading to improved REE extraction and reduced impurity formation.

Keywords: Rare earth elements (REEs); ion adsorption clays; magnesium sulfate; Pourbaix diagram; thermodynamic stability

Abstrak

Elemen Nadir Bumi *(REE)* biasanya diekstrak daripada lempung jerapan ion menggunakan kaedah proses larut resap pertukaran ion, yang melibatkan larutan garam sebagai larutan larut resap. Untuk meningkatkan keberkesanan pengekstrakan *REE*, adalah penting untuk mengekalkan kestabilan termodinamik *REE* dalam larutan garam semasa proses ekstraksi. Oleh itu, pendekatan termodinamik melalui diagram *Pourbaix* telah dijalankan menggunakan perisian *HSC Chemistry 10.0*. Dalam kajian ini, tiga kepekatan *REE* yang paling tinggi dalam lempung jerapan ion- lantanum (La), neodymium (Nd), dan yttrium (Y)- telah diuji menggunakan pelbagai larutan sulfat (ammonium sulfat, magnesium sulfat, dan aluminium sulfat) dengan kepekatan yang berkisar antara 0.05 hingga 0.6 M dan suhu dari 25 hingga 80 °C. Analisis diagram *Pourbaix* menunjukkan bahawa larutan magnesium sulfat adalah larutan larut resap yang paling berkesan, memberikan kestabilan termodinamik maksimum untuk La, Nd, dan Y dalam julat pH 0 hingga 5.8, merentasi semua kepekatan yang diuji, tanpa sebarang pembentukan kimia dalam julat tersebut. Selain itu, kestabilan La, Nd, dan Y didapati menurun apabila suhu larut resap meningkat. Oleh kerana 25°C terbukti sebagai suhu optimum dalam kajian ini, ia menunjukkan bahawa proses larut resap pertukaran ion boleh dijalankan dengan cekap pada suhu ambien, menghapuskan keperluan untuk pemanasan luaran semasa proses ekstraksi. Kesimpulannya, penggunaan magnesium sulfat sebagai larutan larut resap pada suhu ambien meningkatkan kestabilan termodinamik *REE* dalam lempung jerapan ion semasa proses larut resap pertukaran ion, membawa kepada peningkatan ekstraksi *REE* dan pengurangan pembentukan benda asing yang dihasilkan oleh reaksi.

Kata kunci: Unsur nadir bumi, lempung jerapan ion, magnesium sulfat, diagram *Pourbaix*, kestabilan termodinamik

1.0 INTRODUCTION

Rare earth elements (REEs) play a crucial role in modern technologies, encompassing a wide range of industrial applications including the clean energy sector [1, 2]. As the demand for REEs continues to rise, the exploration of potential REE sources has become an utmost priority. Among the potential sources, ion adsorption clays are a highly promising REE source due to their simple extraction methods, low mining costs, and abundant availability. They are also free from high radioactive elements like thorium and uranium [3–5].

REEs in ion adsorption clay primarily exist in the ion-exchangeable phase, which makes up around 60%–90% of the overall REE composition, and predominantly resides on the surface of kaolinite and halloysite [6–8]. Therefore, the most effective way to extract REEs from ion adsorption clay is through ion-exchange leaching using a salt solution, which facilitates REE dissolution. During the ion exchange process, REE^{3+} ions adsorbed onto the clay surface are exchanged with cations from the salt solution, such as NH_4^+. This exchange results in the release of REE^{3+} ions into the external solution, where they are collected as a leachate solution [3], [9], [10]. Equation 1 represents the reaction equation involved in ion-exchange leaching, where M represents the cations that vary based on the specific type of leaching solution employed [3, 4, 11–13].

$$2Clay–REE_{(s)}+3M_2SO_{4(aq)}\rightarrow 2ClayM_3(s)+ REE_2(SO_4)_{3(aq).} \quad (1)$$

Current ion adsorption research is focused on conducting leaching experiments to identify the most effective leaching solutions and optimal conditions, including solution concentration, temperature, and pH, to enhance REE leaching efficiencies Moldoveanu and Papangelakis [14], Burcher-Jones *et al*. [15], and Xu *et al*. [16] found that ammonium sulfate ($NH_4(SO_4)_2$) was the most effective leaching solution, achieving the highest REE leaching efficiency of over 80%. Additionally, Xiao *et al*. [17] and Ran *et al*. [18] discovered that magnesium sulfate ($MgSO_4$) demonstrated similar REE leaching efficiencies to $NH_4(SO_4)_2$ while effectively leaching aluminum, a main impurity in the leachate solution. In line with this research focus, Yang *et al*. [19] introduced a new leaching solution of aluminum sulfate ($Al_2(SO_4)_3$) that had significant REE leaching efficiencies.

In addition to performing leaching experiments, studying thermodynamic stability is crucial for enhancing REE leaching efficiencies. Chemical reactions between REE ions in ion adsorption clay and leaching solution cations often result in the

precipitation of insoluble compounds, impacting overall REE recovery and purity [20]. To address this, Pourbaix diagrams, also known as Eh–pH diagrams, offer a thermodynamic approach by comprehensively evaluating the thermodynamic stability of REEs in under various leaching solutions and conditions at equilibrium [21].

Several studies have investigated the thermodynamic stability of REEs in commercially exploited sources such as bastnaesite, monazite, and xenotime. Lin *et al*. [22] examined the thermodynamic stability of REEs (Ce, La, Nd, and Y) in an acid leaching system using H_2SO_4, HCl, and HNO_3 for the extraction of REEs from bastnaesite, monazite, and xenotime. Similarly, Yahya *et al*. [23] and Kim & Osseo-Asare [24] studied the thermodynamic stability of REEs (Ce, La, and Nd) in a H_2SO_4-based leaching system for the extraction of REEs from monazite. Ahmat *et al*. [25] focused on the thermodynamic stability of yttrium in acid leaching systems using H_2SO_4, HCl, and HNO_3 to represent REE leaching from liquid crystal display (LCD) electronic waste. Meanwhile, Isehaq [26] utilized Pourbaix diagrams to investigate REE extraction from bastnaesite. All the Pourbaix diagrams were generated using HSC Chemistry software. To the best of the authors' knowledge, no study has been conducted to explore the thermodynamic stability of REEs from ion adsorption clay in a salt solution system.

Therefore, this paper aims to construct Pourbaix diagrams (Eh–pH diagram) for three most abundant REEs present in Malaysian ion adsorption clay – lanthanum (La), neodymium (Nd), and yttrium (Y) [10], [27], [28]. La and Nd are selected to represent light rare earth elements (LREE), while yttrium is chosen as a representative of heavy rare earth elements (HREE). The diagrams were developed using HSC Chemistry 10.0 software for three different leaching solutions: ammonium sulfate ($NH_4(SO_4)_2$), magnesium sulfate ($MgSO_4$), and aluminum sulfate ($Al_2(SO_4)_3$), with concentrations ranging from 0.05 to 0.6 M and leaching temperatures between 25 and 80 °C, to observe the thermodynamic behavior of both LREE and HREE under various leaching conditions.

2.0 METHODOLOGY

Construction of Pourbaix diagram using HSC Chemistry 10.0 software. The thermodynamic analysis of REEs was carried out using HSC Chemistry 10.0 software, which involved Pourbaix diagram construction. These diagrams provide information about the stability of REE based on redox potential (Eh) and pH. In these diagrams, the preferred REE species are typically in their soluble ionic forms (REE^{3+}) when the leaching solution is introduced. This region of the diagram provides insights into the pH and Eh conditions where REE^{3+} ions remain in their ionic form within the leaching solution, avoiding undesired reactions or precipitation as insoluble compounds.

HSC Chemistry software uses thermodynamic data and computational algorithms to generate the Pourbaix diagrams, incorporating a database of thermodynamic properties like Gibbs energies (ΔG) and equilibrium constants. To generate the Pourbaix diagram, users define specific details such as the chemical species of REEs and their concentrations, the types of leaching solutions and their concentrations, as well as the pressure and temperature of the system. The software then uses this information to calculate various properties and equilibrium constants relevant to the specified conditions. By analyzing the Gibbs energy (ΔG) values across different ranges of Eh and pH, the software determines the stability boundaries for the different REE species. Subsequently, it plots these stability regions on the diagram, where REEs exist as soluble species (REE^{3+}) and the regions where they may precipitate as insoluble compounds under given leaching conditions. This diagram helps researchers in optimizing the leaching process for efficient REE extraction.

In the Pourbaix diagram, the redox potential (Eh) is usually measured on the Eh scale based on the Standard Hydrogen Electrode (SHE) [29], which indicates the system's ability to gain or lose electrons. Higher potentials (E > 0) promote electron removal, typically near the anode in an electrochemical cell or with certain oxidizing agents. Conversely, lower potentials (E < 0) facilitate electron supply, such as with a cathode electrode or certain reducing agents. Meanwhile, the pH value of a system indicates its capacity to provide protons (H^+) to the species involved. Under acidic conditions (pH < 7), there is a high proton concentration, whereas under alkaline conditions (pH > 7), the proton concentration is low. Figure 1 shows an example of a Pourbaix diagram developed by Lin *et al*. [22] for bastnaesite leaching in H_2SO_4 at 25 °C.

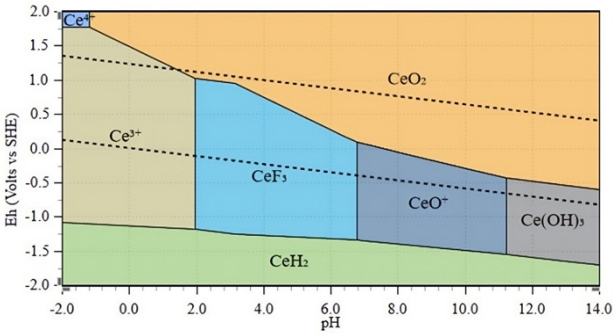

Figure 1 Pourbaix diagram for bastnaesite leaching in H_2SO_4 at 25 °C

From Figure 1, the line in the Pourbaix diagram represents the chemical reactions [24, 26]:

- Horizontal lines: Reactions that are involved with electrons but are independent of pH.

- Vertical lines: Reactions that are involved with H^+ and OH^- ions but are independent of electrons.
- Diagonal lines: Reactions that are involved with both electrons and H^+ and OH^- ions.
- Dotted lines: The chemical stability area of water.

Table 1 presents the input parameters obtained from relevant literature sources, which were used to generate the Pourbaix diagram. The selected parameters were based on studies that investigated the effect of these parameters on the leaching efficiencies of REEs through experimental work. The thermodynamic analysis was divided into two parts. In the first part, the study examined how the stability of La, Nd, and Y was affected by different concentrations of $(NH_4)_2SO_4$, $MgSO_4$, and $Al_3(SO_4)_3$ at 25 °C. After determining the minimum concentration, which reflects the most thermodynamic stable condition, the second part of the analysis explored the impact of varying leaching temperatures on the stability of La, Nd, and Y in $(NH_4)_2SO_4$, $MgSO_4$, and $Al_3(SO_4)_3$.

The generation of Pourbaix diagrams has certain limitations, as it can represent only a single element in a single solvent, excluding multiple elements and potential impurities, which may introduce uncertainties due to the assumptions made during diagram construction. Since this study focuses on diagram generation, further validation with experimental data is needed to gain a more comprehensive understanding of the thermodynamic behavior under specific leaching conditions.

Table 1 Input parameter for Pourbaix diagram generation

Parameters	Input parameters	Literature sources
REE concentration (Molality)	• Lanthanum (La): 0.005 m • Neodymium (Nd): 0.004 m • Yttrium (Y): 0.004 m	[28], [27], [10]
Type of leaching solution	• Ammonium sulfate, $(NH_4)_2SO_4$ • Magnesium sulfate, $MgSO_4$ • Aluminum sulfate, $Al_2(SO_4)_3$	[14], [15], [16], [17], [18], [19]
Leaching solution concentration (M)	• 0.05, 0.1, 0.15, 0.2, 0.3, 0.35, 0.4, 0.45, 0.5, 0.55, 0.6	[30]
Leaching temperature (°C)	• 25, 30, 40, 50, 60, 70, 80	[31]

3.0 RESULTS AND DISCUSSION

Effect of leaching solution concentration on REE stability. The leaching solution concentration directly impacts thermodynamic stability of REEs during the leaching process. Higher leaching solution concentrations influence the pH and redox potential (Eh) of the system, affecting the stability of different REE species. At certain concentrations, the leaching solution promotes the formation soluble ionic forms (REE^{3+}) without causing undesired reactions or the precipitation of insoluble compounds, thereby enhancing extraction efficiency. However, excessive concentrations of the leaching solution can precipitate REEs into insoluble compounds, reducing their recovery and purity [32]. Thus, carefully controlling the leaching solution concentration is essential for optimizing REE extraction processes and obtaining high yields of valuable REE products.

1. Thermodynamic stability of La, Nd, and Y in $(NH_4)_2SO_4$ solution.

The maximum thermodynamic stability region for La^{3+} was observed at 25 °C between the concentration range of 0.05 to 0.25 M of $(NH_4)_2SO_4$ solution and under acidic conditions, with a pH range of 0 to 5.8. Figure 2 illustrates Pourbaix diagrams for the La–S–N system in 0.05 M $(NH_4)_2SO_4$ at 25 °C, as well as for concentrations of 0.1 M, 0.15 M, 0.2 M, and 0.25 M. When the concentration of $(NH_4)_2SO_4$ solution increased to 0.3 M, the thermodynamic stability region of La^{3+} decreased due to the formation of lanthanum nitrate complex ($LaNO_3^{2+}$), as depicted in Figure 3. The thermodynamic stability region of $LaNO_3^{2+}$ expanded when the concentration of $(NH_4)_2SO_4$ solution increased from 0.35 to 0.6 M while the stability region of La^{3+} remained consistent. This effect is depicted in Figure 4, representing the Pourbaix diagram for the La–S–N system in a 0.6 M $(NH_4)_2SO_4$ solution.

$LaNO_3^{2+}$ forms when La^{3+} reacts with nitrate ions (NO_3^-), as shown in Equation 2. The presence of NO_3^- in the system can be attributed to the nitrification process in which NH_4^+ ions are oxidized to NO_2^- ions, followed by further oxidation to NO_3^- ions by nitrifying bacteria [31–33]. The overall nitrification process is represented by Equation 3. Consequently, as $(NH_4)_2SO_4$ concentration increased, NH_4^+ concentration also increased, providing more opportunities for NH_4^+ ions to be oxidized by nitrifying bacteria. This led to a higher production of NO_3^- ions, ultimately facilitating the formation of more $LaNO_3^{2+}$ ions. Nitrification plays a vital role in the natural nitrogen cycle, in which nitrifying bacteria thrive in the presence of ammonia ions [36].

$$La^{3+} + 2NO_3^- \rightarrow LaNO_3^{2+} \quad (2)$$

$$2NH_4^+ + 3O_2^- \rightarrow 2NO_3^- + 2H_2O \quad (3)$$

The maximum thermodynamic stability region for Nd^{3+} was observed within the concentration range of 0.05 M only under acidic conditions with a pH range of 0 to 5, as depicted in Figure 5. However, when the concentration increased to 0.1 M, the thermodynamic stability region of Nd^{3+} decreased due to the formation of neodymium nitrate complex

($NdNO_3^{2+}$), as illustrated in Figure 6. The thermodynamic stability region of $NdNO_3^{2+}$ expanded when the concentration of $(NH_4)_2SO_4$ solution increased from 0.1 to 0.6 M while the stability region of Nd^{3+} remained consistent. This effect is depicted in Figure 7, representing the Pourbaix diagram for the Nd–S–N system in a 0.6 M $(NH_4)_2SO_4$ solution. $NdNO_3^{2+}$ forms when Nd^{3+} reacts with NO_3^-, in which the presence of NO_3^- in the system is due to the nitrification process, as explained earlier.

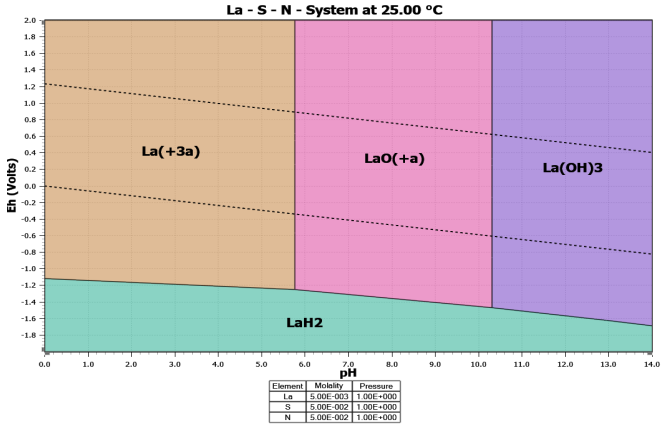

Figure 2 Pourbaix diagrams of the La–S–N system in 0.05 M $(NH_4)_2SO_4$ at 25 °C

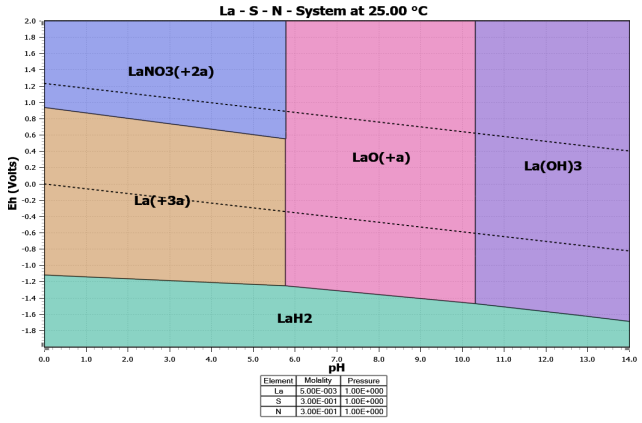

Figure 3 Pourbaix diagrams of the La–S–N system in 0.3 M $(NH_4)_2SO_4$ at 25 °C

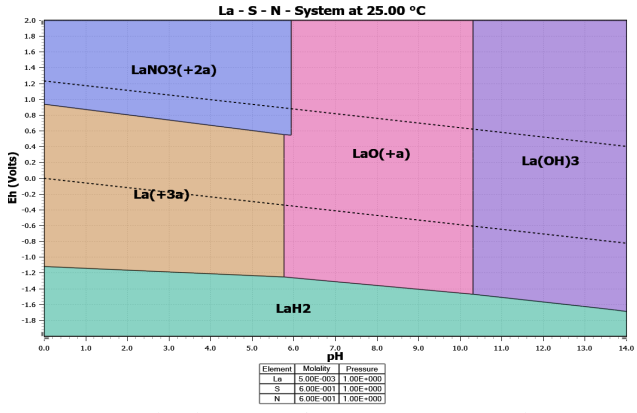

Figure 4 Pourbaix diagrams of the La–S–N system in 0.6 M $(NH_4)_2SO_4$ at 25 °C

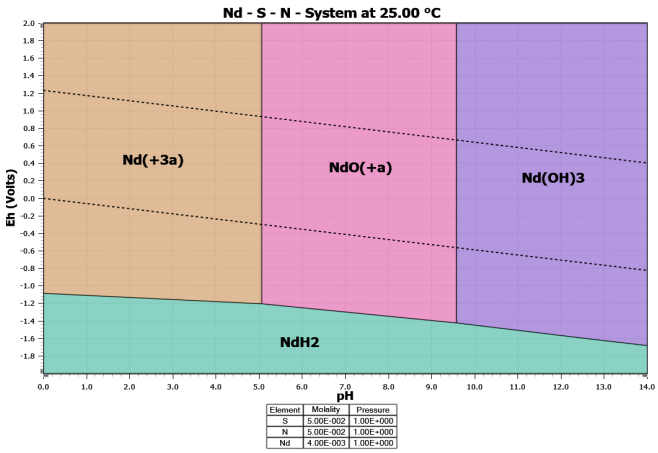

Figure 5 Pourbaix diagrams of the Nd–S–N system in 0.05 M $(NH_4)_2SO_4$ at 25 °C

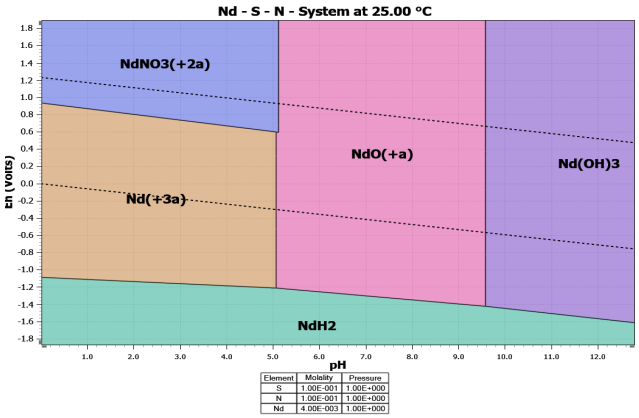

Figure 6 Pourbaix diagrams of the Nd–S–N system in 0.1 M $(NH_4)_2SO_4$ at 25 °C

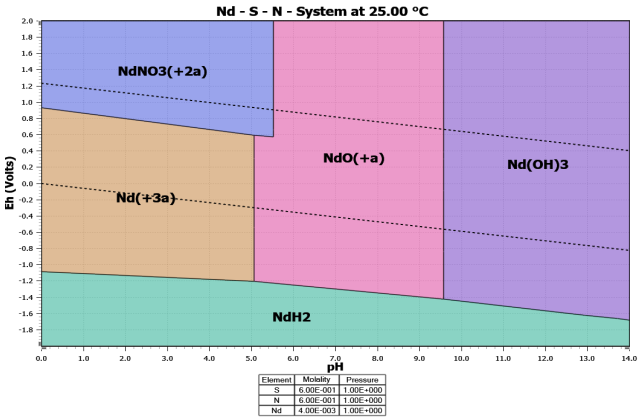

Figure 7 Pourbaix diagrams of the Nd–S–N system in 0.6 M $(NH_4)_2SO_4$ at 25 °C

Additionally, the stability region for Y^{3+} is maintained across the entire concentration range from 0.05 to 0.6 M under a pH range of 0 to 4.2. This suggests that Y^{3+} forms stable ionic species that are less influenced by changes in concentration. Figure 8 depicts the Pourbaix diagram illustrating the Y–S–N system in a 0.05 M solution of $(NH_4)_2SO_4$, as well as for concentrations ranging from 0.1 M to 0.6 M.

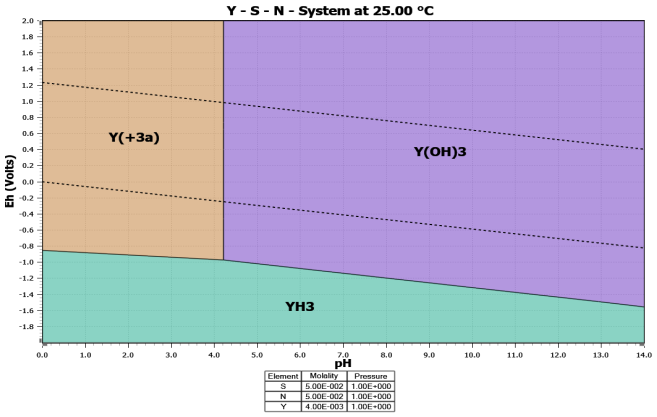

Figure 8 Pourbaix diagrams of the Y–S–N system in 0.05 M $(NH_4)_2SO_4$ at 25 °C

The thermodynamic stability region of La^{3+}, Nd^{3+}, and Y^{3+} ions in $(NH_4)_2SO_4$ solution was observed to be stable within an acidic pH range between 0 to 5.8. These results were supported with the findings of Chai *et al*. (2020), who determined that a pH of 4.0 was optimal for the experimental leaching of REEs using an ammonium solution. This preference for acidic pH was attributed to the increased solubility of REE ion in the leaching solution under such conditions [32]. The acidic pH of the leaching solution played a crucial role in keeping the REEs in a dissolved state as ions, preventing their precipitation as insoluble compounds. In addition, by maintaining the pH in the acidic range, certain competing ions in the clay such as aluminum (Al) and iron (Fe) tended to remain in their less soluble forms, thereby reducing their interference with REE extraction from the clay and facilitating for more effective separation and extraction of REEs [38].

2. Thermodynamic stability of La, Nd, and Y in $MgSO_4$ solution.

The maximum thermodynamic stability regions for La^{3+}, Nd^{3+}, and Y^{3+} were consistently observed in $MgSO_4$ solutions across all concentrations, ranging from 0.05 to 0.6 M, at a temperature of 25°C. Figure 9 depicts the Pourbaix diagrams, showing the thermodynamic stability region of La^{3+} at 0.05 M within the pH range of 0 to 5.8, as well for concentration ranging from 0.1 M to 0.6 M. Similarly, Figure 10 illustrates Nd^{3+} at 0.05 M within the pH range of 0 to 5 while Figures 11 for Y^{3+} at 0.05 M within the pH range of 0 to 4.2.

The consistent maximum thermodynamic stability region observed for La^{3+}, Nd^{3+}, and Y^{3+} in $MgSO_4$ solutions across various concentrations could be primarily attributed to the presence of Mg^{2+} ions in the leaching solution. These findings were supported by Chen *et al*. [31], who demonstrated that the use of a 0.23 M $MgSO_4$ leaching solution achieved a higher REE leaching efficiency of 96.19% after the application of the second stage leaching, compared to only 93.87% with a 0.23 M $(NH_4)_2SO_4$ solution. In contrast to NH_4^+ ions in $(NH_4)_2SO_4$ solution, Mg^{2+} ions possess a higher charge, which allows them to contribute significantly to the ionic strength of the solution. Consequently, this increase in ionic strength led to a reduction in the activity coefficient of La^{3+}, Nd^{3+}, and Y^{3+}. This reduction in the activity coefficient was a crucial factor in ensuring La^{3+}, Nd^{3+}, and Y^{3+} were maintained in ionic forms and prevented undesired reactions or precipitation of insoluble compounds.

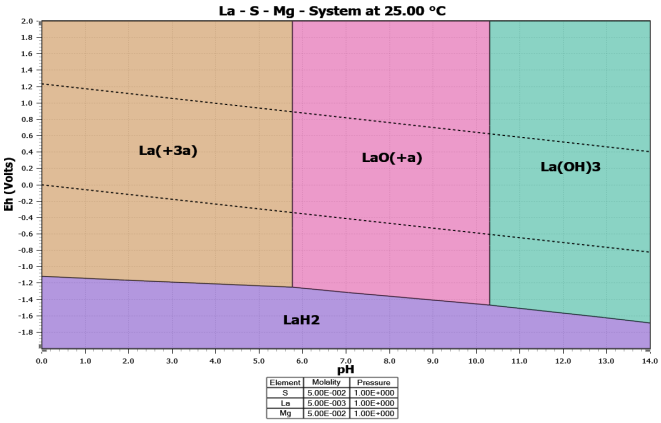

Figure 9 Pourbaix diagrams of the La–S–Mg system in 0.05 M $MgSO_4$ at 25 °C

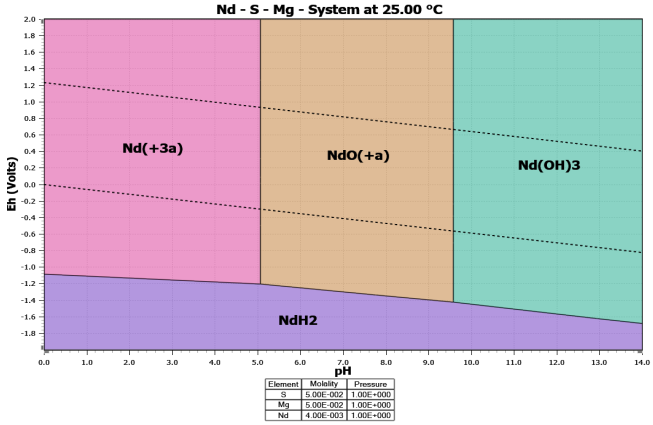

Figure 10 Pourbaix diagrams of the Nd–S–Mg system in 0.05 M $MgSO_4$ at 25 °C

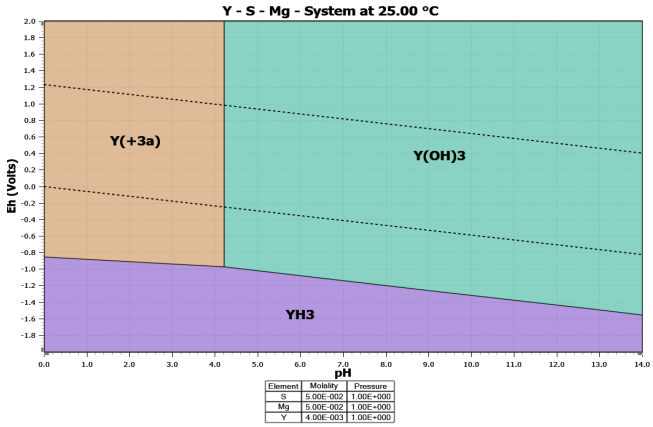

Figure 11 Pourbaix diagrams of the Y–S–Mg system in 0.05 M $MgSO_4$ at 25 °C

3. Thermodynamic stability of La, Nd, and Y in $Al_2(SO_4)_3$ solution.

The thermodynamic stability region of La^{3+} in $Al_2(SO_4)_3$ leaching solution at 25 °C was represented by a little formation of $LaSO_4^+$ complex species across all the concentrations ranging from 0.05 to 0.6 M. Figure 12 represents the Pourbaix diagrams showing the thermodynamic stability region of La^{3+} at 0.05 M within the pH range of 0 to 5.8. The formation of $LaSO_4^+$ complex species is due to the formation of a coordination complex between La^{3+} and SO_4^{2-} ions. Coordination complexes are compounds in which a central metal ion is surrounded by ligands (atoms, ions, or molecules) that donate electron pairs to the metal ion, forming coordinate bonds [39]. In this case, the SO_4^{2-} ion functions as a ligand, that donate electron pairs to La^{3+} resulting the formation of a complex of +1 charge which is $LaSO_4^+$.

However, when the concentration of $Al_2(SO_4)_3$ increased, more sulfate ions (SO_4^{2-}) were available to react with La^{3+}, promoting the formation of $LaSO_4^+$ species, resulting to a slight expansion of the stability region of $LaSO_4^+$. This effect is illustrated in Figure 13 for La-S-Al system in 0.6 M $Al_2(SO_4)_3$. The thermodynamic stability region of La^{3+} in $Al_2(SO_4)_3$ solution decreased, mainly due to the increased formation of $LaSO_4^+$ within the pH range of 5-6. The presence of complex species like $LaSO_4^+$ can influence the purity of REE and may affect REE extraction efficiency.

Similarly, the thermodynamic stability of Nd^{3+} in $Al_2(SO_4)_3$ is affected by the formation of $Nd_2(SO_4)_3{\cdot}8H_2O$. Figure 14 represents the Pourbaix diagrams for Nd^{3+} in $Al_2(SO_4)_3$ at 0.05 M, within the acidic pH range of 0 to 5. The formation of $Nd_2(SO_4)_3$ indicates that two Nd^{3+} ions are reacted with three SO_4^{2-} ions. This formation is hydrated, meaning that it is associated with water molecules, resulting in the formation of $Nd_2(SO_4)_3{\cdot}8H_2O$.

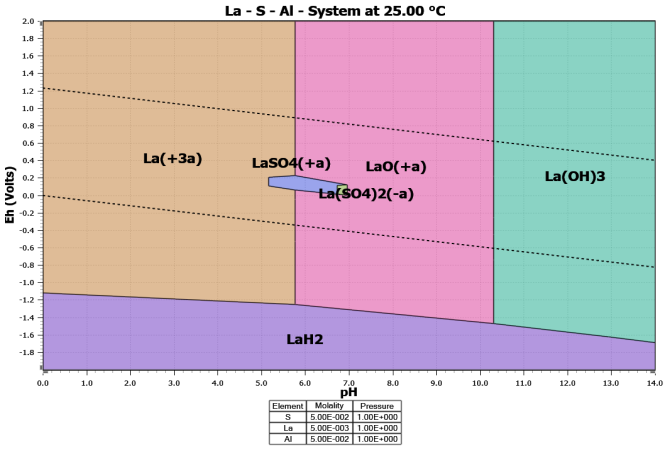

Figure 12 Pourbaix diagrams of the La–S–Al system in 0.05 M $Al_2(SO_4)_3$ at 25 °C

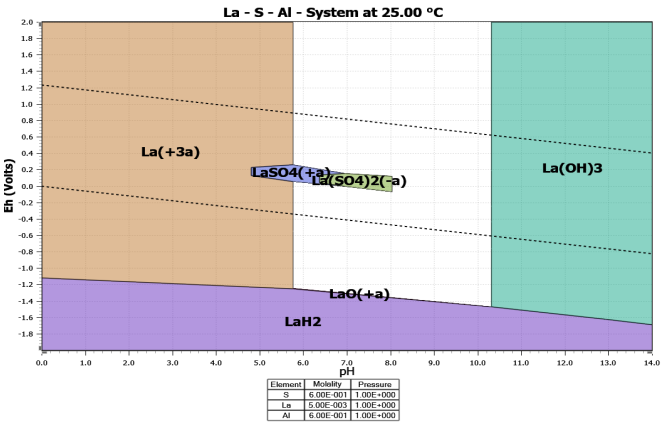

Figure 13 Pourbaix diagrams of the La–S–Al system in 0.6 M $Al_2(SO_4)_3$ at 25 °C

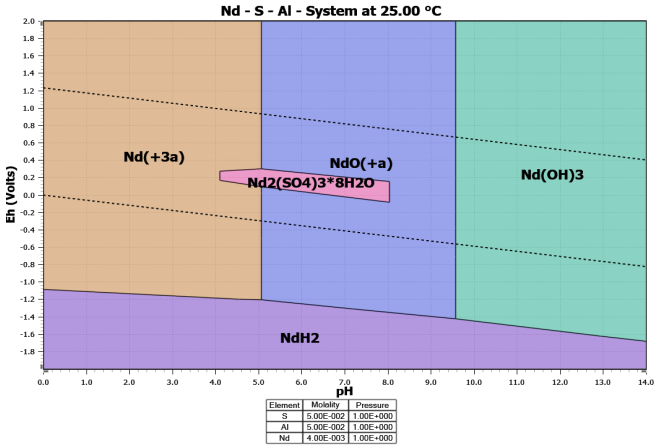

Figure 14 Pourbaix diagrams of the Nd–S–Al system in 0.05 M $Al_2(SO_4)_3$ at 25 °C

In this compound, water molecules are physically trapped within the crystalline lattice and present as part of the crystal structure. As the concentration of $Al_2(SO_4)_3$ increased, more SO_4^{2-} ions became available, promoting the formation of the $Nd_2(SO_4)_3{\cdot}8H_2O$, and thus expanding its stability region. Consequently, this expansion led a decrease thermodynamic stability region of Nd^{3+} in $Al_2(SO_4)_3$ solution. This effect is illustrated in Figure 15 for Nd-S-Al system in 0.6 M $Al_2(SO_4)_3$.

In contrast, the thermodynamic stability region of Y^{3+} in $Al_2(SO_4)_3$ solution remained consistent across all concentrations ranging from 0.05 to 0.6 M and within the pH range of 0 to 4.2. This effect is depicted in Figure 16 for Y-S-Al system in 0.05 M $Al_2(SO_4)_3$. It highlights the stable nature of Y^{3+} in the $Al_2(SO_4)_3$ where it did not form significant complexes or undergo chemical reactions with the SO_4^{2-} ions in the leaching solution.

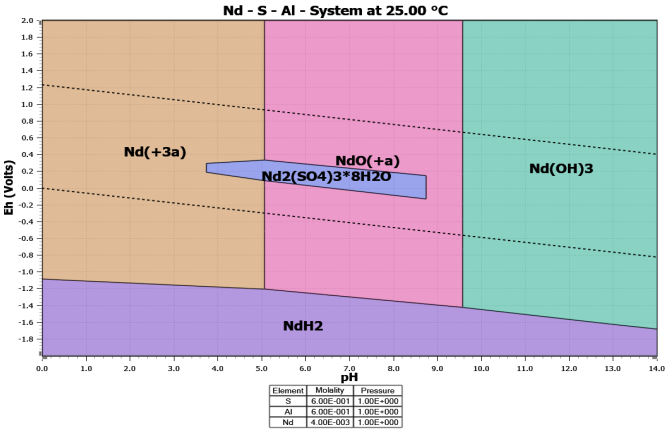

Figure 15 Pourbaix diagrams of the Nd–S–Al system in 0.6 M $Al_2(SO_4)_3$ at 25 °C

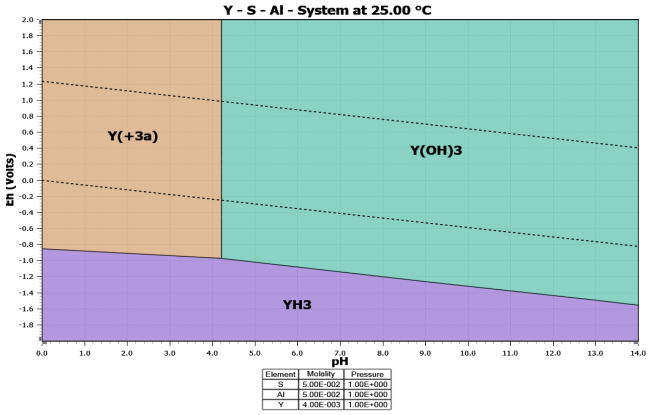

Figure 16 Pourbaix diagrams of the Y–S–Al system in 0.05 M $Al_2(SO_4)_3$ at 25 °C

A summary of the findings on the effect of leaching solution concentration on the thermodynamic aqueous stability of La, Nd, and Y in three different types of leaching solutions revealed that the most effective leaching solution was $MgSO_4$. This solution consistently exhibited the maximum thermodynamic stability region for La, Nd, and Y across all tested concentrations without the formation of unwanted reactions within their stability region. The stability trend of La, Nd, and Y in the three leaching solutions followed a consistent pattern, with increasing stability observed in the order of La > Nd > Y for all the concentrations tested from 0.05 to 0.6 M.

Effect of leaching temperature on REE stability. The thermodynamic stability region of La^{3+}, Nd^{3+}, and Y^{3+} was investigated at a leaching temperature range of 25 to 80 °C by using $(NH_4)_2SO_4$, $MgSO_4$, and $Al_2(SO_4)_3$ leaching solutions. In this study, the minimum concentration of 0.05M was selected for each type of leaching solution which represents the most thermodynamically stable condition. With the increasing temperature, the thermodynamic stability regions of La^{3+}, Nd^{3+}, and Y^{3+} in the three leaching solutions decreased. The REE^{3+} region underwent a noticeable shift, leading to a reduction in the width of its stability region. Pourbaix diagrams, represented by Figure 17 and Figure 18 elucidates the trend of decreasing thermodynamic stability region for La^{3+} ions in the $MgSO_4$ leaching solution at 0.05 M, as the temperature increased from 25 to 80 °C, as well for Nd and Y. The same trend was also observed in the $(NH_4)_2SO_4$ and $Al_2(SO_4)_3$ solution The thermodynamic stability increasing in the order of La > Nd > Y for all the leaching temperatures tested from 25 to 80 °C.

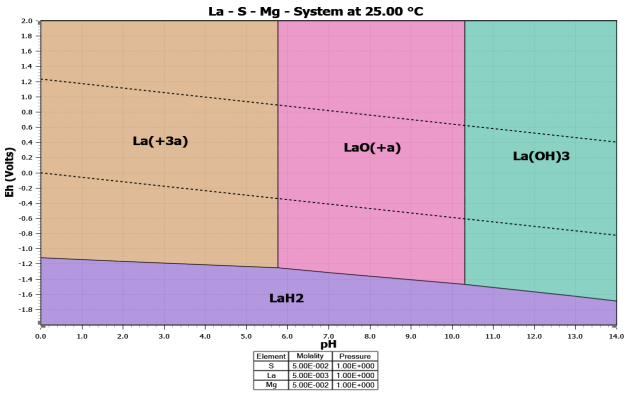

Figure 17 Pourbaix diagrams of the La–S–Mg system in 0.05 M $MgSO_4$ at 25 °C

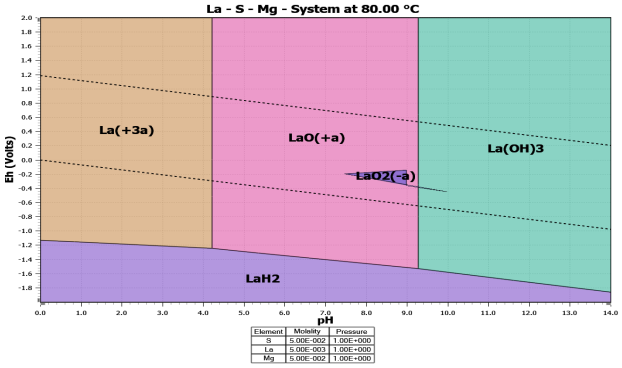

Figure 18 Pourbaix diagrams of the La–S–Mg system in 0.05 M $MgSO_4$ at 80°C

As the temperature rises, the thermal energy within the system increases, resulting in greater molecular motion. This increased molecular motion facilitates more frequent collisions between REE ions and other ions present in the leaching solution. Consequently, the reaction rates between ions and surrounding molecules or ions increase, leading to increased occurrences of complexation, precipitation, and redox reactions. Figures 18 shows the increased formation of insoluble compounds such as $La(OH)_3$ as the temperature increased to 80 °C. These precipitation reactions exemplify the generation of insoluble compounds in the leaching solution. Equation 4 illustrates a precipitation reaction wherein La^{3+} ions react with hydroxide ions (OH^-) to form $La(OH)_3$.

$La^{3+} + 3\ OH^- \rightarrow La(OH)_3$. 4

Figure 18 also exhibit the increased formation of LaO^+ due to complexation reactions when the temperature increased to 80 °C . In these reactions, La^{3+} ions coordinate with ligands, such as water (H_2O), which can donate lone pairs of electrons. The interaction between the metal ions and the water ligands creates stable complexes, facilitated by the establishment of coordination bonds [40, 41]. Overall, these observations highlight the significant impact of temperature on the thermodynamic stability of REE ions in the leaching solution. From this study, a leaching temperature of 25 °C has been determined to be optimal in this study, enabling ion-exchange leaching to be conducted at ambient temperature without requiring additional heat. The findings were consistent with the experimental data from Chen *et al*. [31], who suggested using room temperature for column leaching REEs from ion adsorption clay using $MgSO_4$ solution, while Yanfei *et al*. [42] recommended 25 °C for the same leaching process since the leaching efficiency of REEs was virtually constant after 30 minutes in the temperature range used.

Thermodynamic Data. In the context of chemical reactions, ΔG represents the difference in Gibbs energy between the products and the reactants. It determines whether a chemical reaction can proceed spontaneously or whether an external energy input is needed [43]. If ΔG is negative ($\Delta G < 0$), the reaction is exergonic and occurs spontaneously, releasing energy. On the other hand, if ΔG is positive ($\Delta G > 0$), the reaction is endergonic and does not occur spontaneously without the input of energy. In the process of constructing a Pourbaix diagram, the stability boundaries on the coordinate axes were established by analyzing the Gibbs energy (ΔG) of various equilibria. The ΔG data was based on the enthalpy, entropy, and heat capacity values taken from the HSC Chemistry 10.0 software database [23]. Table 2 shows the ΔG values for La^{3+}, Nd^{3+}, and Y^{3+} ions at different temperatures.

At 25 °C, La^{3+}, Nd^{3+}, and Y^{3+} exhibited the smallest ΔG values among the considered temperatures. This negative ΔG value signifies energetically favorable formation, leading to increased stability of these ions in the leaching solution. As a result, at 25 °C, all three REE ions (La^{3+}, Nd^{3+}, and Y^{3+}) are thermodynamically stable. This is further supported by the maximum stability region of La^{3+}, Nd^{3+}, and Y^{3+} on the Pourbaix diagram, which corresponds to 25 °C. Moreover, the lower ΔG value for La^{3+} compared to Nd^{3+} and Y^{3+} at any given temperature suggests that La^{3+} is the most stable among the three REEs under those specific conditions. This is evident from the Pourbaix diagram, where La^{3+} exhibits the widest stability region spanning from pH 0 to 5.8, whereas Nd^{3+} has a stability region from pH 0 to 5, and Y^{3+} from pH 0 to 4.2 in the three types of leaching solution.

Table 2 Thermodynamic data from HSC Chemistry 10.0 software

Temperature (°C)	$\Delta G°_T$ (kcal/mol)		
	La^{3+}	Nd^{3+}	Y^{3+}
25	-163.997	-160.205	-163.788
30	-163.912	-160.106	-163.668
40	-163.735	-159.897	-163.427
50	-163.549	-159.678	-163.184
60	-163.355	-159.449	-162.938
70	-163.153	-159.211	-162.690
80	-162.943	-158.964	162.440

4.0 CONCLUSION

This study employed a thermodynamic stability approach using Pourbaix diagrams generated with HSC Chemistry 10.0 software to investigate REE behavior in ion adsorption clays. The findings provide valuable insights into optimizing REE extraction under various leaching conditions. Among the leaching solutions tested, $MgSO_4$ exhibited the most favorable thermodynamic stability for La, Nd, and Y across all concentrations (0.05–0.6 M) within an acidic pH range of 0–5.8, with any unwanted chemical species forming in this region. Temperature was found to significantly influence REE stability: as the temperature increased, the thermodynamic stability regions of La^{3+}, Nd^{3+}, and Y^{3+} narrowed, with a noticeable shift in the REE zones. The most optimal condition was observed at 25 °C, allowing ion-exchange leaching to occur at ambient temperature without the need for additional heating, thus supporting energy-efficient processing. These results have important implications for the design of more efficient and sustainable REE leaching strategies, particularly from ion adsorption clay sources. The Pourbaix diagram approach serves as a predictive tool for selecting appropriate leaching conditions and can guide future experimental validation and process optimization in rare earth extraction research.

Acknowledgement

The authors would like to thank the Ministry of Higher Education (MoHE) Malaysia for providing financial support under Fundamental Research Grant Scheme No. FRGS/1/2021/TK0/UMP/02/26 (University reference RDU210130) and Universiti Malaysia Pahang Al-Sultan Abdullah for laboratory facilities.

Conflicts of Interest

The authors declare that there is no conflict of interest regarding the publication of this paper.

References

[1] Filho, W. L., Kotter, R., Özuyar, P.G., Abubakar, I. R., Eustachio, J. H. P. P., Matandirotya, N. R. 2023. Understanding Rare Earth Elements as Critical Raw Materials. *Sustain*. 15. https://doi.org/10.3390/su15031919.

[2] Charalampides, G., Vatalis, K. I., Apostoplos, B., Ploutarch-Nikolas, B. 2015. Rare Earth Elements: Industrial Applications and Economic Dependency of Europe. *Procedia Econ. Financ*. 24: 126–135. https://doi.org/10.1016/S2212- 5671(15)00630-9.

[3] Feng, X., Onel, O., Council-Troche, M., Noble, A., Yoon, R. H., Morris, J. R. 2021. A Study of Rare Earth Ion-adsorption Clays: The Speciation of Rare Earth Elements on Kaolinite at Basic pH. *Appl. Clay Sci.* 201: 105920. https://doi.org/10.1016/j.clay.2020.105920.

[4] Yaraghi, A., Baharun, N., Ariffin, K. S. 2019. A Short Review on REE Recovery from Ion-adsorption Clays. *Asp. Min. Miner. Sci.* 2(5): 550. https://doi.org/ 10.31031/amms.2019.02.000550.

[5] Borst, A., Smith, M., Finch, A., Estrade, G., Villanova-de-Benavent, C., Nason, P., Marquis, E., Horsburgh, N., Goodenough, K., Xu, C., Kynicky, J., Geraki, K. 2020. Adsorption of Rare Earth Elements in Regolith-hosted Clay Deposits. *Nat. Commun*. 11. https://doi.org/10.1038/s41467-020-17801-5.

[6] Khairulanuar, K. A., Segeran, L., Jabit, N., Ismail, S., Ibrahim, I., Ariffin, K. S. 2022. Characterisation of Rare Earth Elements from Malaysian Ion-adsorption Clay. *Mater. Today Proc*. 66: 3049–3052. https://doi.org/10.1016/j.matpr.2022.07.336.

[7] Huang, J., Tan, W., Liang, X., He, H., Ma, L., Bao, Z., Zhu, J. 2021. REE Fractionation Controlled by REE Speciation during Formation of the Renju Regolith-hosted REE Deposits in Guangdong Province, South China. *Ore Geol. Rev*. 134: 104172. https://doi.org/10.1016/j.oregeorev.2021.104172.

[8] Hoshino, M., K. Sanematsu, and Y. Watanabe. 2016. REE Mineralogy and Resources. In *Handbook on the Physics and Chemistry of Rare Earths*, 129–291. Amsterdam: Elsevier B.V. https://doi.org/10.1016/bs.hpcre.2016.03.006.

[9] Estrade, G., Marquis, E., Smith, M., Goodenough, K., Nason, P. 2019. REE Concentration Processes in Ion Adsorption Deposits: Evidence from the Ambohimirahavavy Alkaline Complex in Madagascar. *Ore Geol. Rev*. 112: 103027. https://doi.org/10.1016/j.oregeorev.2019.103027.

[10] Sobri, N. A., Yunus, M. Y. B. M., Harun, N. 2023. A Review of Ion Adsorption Clay as a High Potential Source of Rare Earth Minerals in Malaysia. *Mater. Today Proc*. https://doi.org/10.1016/j.matpr.2023.03.513.

[11] Godang, S., A. Idrus, Fadlin Priadi, and N. I. Basuki. 2019. Characteristics of Rare Earth Elements in Volcanic Regolith on Drill Core in Western Sulawesi, Indonesia. *Asian Journal of Applied Sciences*. 7: 435–450. https://doi.org/10.24203/ajas.v7i4.5873.

[12] Moldoveanu, G., and V. Papangelakis. 2016. An Overview of Rare-Earth Recovery by Ion-Exchange Leaching from Ion-Adsorption Clays of Various Origins. *Mineralogical Magazine*. 80: 63–76. https://doi.org/10.1180/minmag.2016.080.051.

[13] Zhang, Z., Q. Jia, and W. Liao. 2015. Progress in the Separation Processes for Rare Earth Resources. In *Handbook on the Physics and Chemistry of Rare Earths*, 287–376. https://doi.org/10.1016/B978-0-444-63483-2.00004-1.

[14] Moldoveanu, G., and V. Papangelakis. 2012. Recovery of Rare Earth Elements Adsorbed on Clay Minerals: I. Desorption Mechanism. *Hydrometallurgy*. 117–118: 71–78. https://doi.org/10.1016/j.hydromet.2012.02.007.

[15] Burcher-Jones, C., S. Mkhize, M. Becker, R. Ram, and J. Petersen. 2018. Study of the Deportment of REEs in Ion Adsorption Clays Towards the Development of an In Situ Leaching Strategy. In *Proceedings of the First Global Conference on Extractive Metallurgy*, in *The Minerals, Metals & Materials Series*, 2429–2439. https://doi.org/10.1007/978-3-319-95022-8_205.

[16] Xu, Q., Y. Sun, L. Yang, C. Li, X. Zhou, W. Chen, and Y. Li. 2019. Leaching Mechanism of Ion-Adsorption Rare Earth by Monovalent Cation Electrolytes and the Corresponding Environmental Impact. *Journal of Cleaner Production*. 211: 566–573. https://doi.org/10.1016/j.jclepro.2018.11.112.

[17] Xiao, Y. F., Y. Y. Chen, Z. Y. Feng, X. W. Huang, L. Huang, Z. Q. Long, and D. L. Cui. 2015. Leaching Characteristics of Ion-Adsorption Type Rare Earths Ore with Magnesium Sulfate. *Transactions of Nonferrous Metals Society of China (English Edition)*. 25: 3784–3790. https://doi.org/10.1016/S1003-6326(15)64022-5.

[18] Ran, X., Z. Ren, H. Gao, R. Zheng, and J. Jin. 2017. Kinetics of Rare Earth and Aluminum Leaching from Kaolin. *Minerals*. 7. https://doi.org/10.3390/min7090152.

[19] Yang, L., C. Li, D. Wang, F. Li, Y. Liu, X. Zhou, M. Liu, X. Wang, and Y. Li. 2019. Leaching Ion Adsorption Rare Earth by Aluminum Sulfate for Increasing Efficiency and Lowering the Environmental Impact. *Journal of Rare Earths*. 37: 429–436. https://doi.org/10.1016/j.jre.2018.08.012.

[20] Chivavava, J., J. Petersen, and A. E. Lewis. 2024. Comparing the Recovery of Rare Earth Elements from Ion-Adsorption Clay Leach Solutions Using Various Precipitants. *Journal of the Southern African Institute of Mining and Metallurgy*. 124(12): 737–746. https://doi.org/10.17159/2411-9717/730/2024.

[21] Roh, Y., R. J. Lauf, A. D. McMillan, C. Zhang, C. J. Rawn, J. Bai, and T. J. Phelps. 2001. Microbial Synthesis and the Characterization of Metal-Substituted Magnetites. *Solid State Communications*. 118: 529–534. https://doi.org/10.1016/S0038-1098(01)00146-6.

[22] Lin, P., X. Yang, J. M. Werner, and R. Q. Honaker. 2021. Application of Eh-pH Diagrams on Acid Leaching Systems for the Recovery of REEs from Bastnaesite, Monazite and Xenotime. *Metals (Basel)*. 11. https://doi.org/10.3390/met11050734.

[23] Yahya, F. Nasuha, L. Nadirah Mat Suli, W. Hanisah Wan Ibrahim, and R. Abdul Rasid. 2019. Thermodynamic Evaluation of the Aqueous Stability of Rare Earth Elements in Sulfuric Acid Leaching of Monazite through Pourbaix Diagram. *Materials Today: Proceedings*. 19: 1647–1656. https://doi.org/10.1016/j.matpr.2019.11.193.

[24] Kim, E., and K. Osseo-Asare. 2012. Aqueous Stability of Thorium and Rare Earth Metals in Monazite Hydrometallurgy: Eh–pH Diagrams for the Systems Th–, Ce, La–, Nd– (PO4)–(SO4)–H2O at 25°C. *Hydrometallurgy*. 113–114: 67–78. https://doi.org/10.1016/j.hydromet.2011.12.007.

[25] Ahmat, F., M. Y. Mohd Yunus, B. Abd Aziz, and A. Hisyam. 2018. Application of Thermodynamic Modelling and Experimental Investigation of Leaching Yttrium from Liquid Crystal Display. *Journal of Chemical Engineering and Industrial Biotechnology*. 3(1): 17–25. https://doi.org/10.15282/jceib.v3i.

[26] Isehaq, S. A.-N. 2015. *Application of Pourbaix Diagrams in the Hydrometallurgical Processing of Bastnasite*. Master's thesis, The Pennsylvania State University.

[27] Tohar, S. Z., and M. Y. M. Yunus. 2020. Mineralogy and BCR Sequential Leaching of Ion-Adsorption Type REE: A Novelty Study at Johor, Malaysia. *Physics and Chemistry of the Earth*. 120: 102947. https://doi.org/10.1016/j.pce.2020.102947.

[28] A., K. S. Ariffin, and N. Baharun. 2020. Comparison of Characteristics and Geochemical Behaviors of REEs in Two Weathered Granitic Profiles Generated from Metamictized Bedrocks in Western Peninsular Malaysia. *Journal of Asian Earth Sciences*. 199: 104385. https://doi.org/10.1016/j.jseaes.2020.104385.

[29] Huang, Hsin-Hsiung. 2016. The Eh-pH Diagram and Its Advances. *Metals*. 6(1): Article 23. https://doi.org/10.3390/met6010023.

[30] Yin, Shuang, Jiang Pei, Feng Jiang, Shun Li, Jian Peng, Liang Zhang, Shuang Ju, and Chinnadurai Srinivasakannan. 2018. Ultrasound-Assisted Leaching of Rare Earths from the Weathered Crust Elution-Deposited Ore Using Magnesium Sulfate without Ammonia-Nitrogen Pollution. *Ultrasonics Sonochemistry*. 41(January): 156–162. https://doi.org/10.1016/j.ultsonch.2017.09.028.

[31] Chen, Kai, Jiang Pei, Shuang Yin, Shun Li, Jian Peng, and Liang Zhang. 2018. Leaching Behaviour of Rare Earth Elements from Low-Grade Weathered Crust Elution-Deposited Rare Earth Ore Using Magnesium Sulfate. *Clay Minerals*. 53(4): 505–514. https://doi.org/10.1180/clm.2018.37.

[32] Arrachart, G., J. Couturier, S. Dourdain, C. Levard, and S. Pellet-Rostaing. 2021. Recovery of Rare Earth Elements (REEs) Using Ionic Solvents. *Processes*. 9(7): 1202. https://doi.org/10.3390/pr9071202.

[33] González-Tineo, P., A. Aguilar, A. Reynoso, U. Durán, M. Garzón-Zúñiga, E. Meza-Escalante, L. Álvarez, and D. Serrano. 2022. Organic Matter Removal in a Simultaneous Nitrification–Denitrification Process Using Fixed-Film System. *Scientific Reports*. 12: 1882. https://doi.org/10.1038/s41598-022-05521-3.

[34] Salama, Y., M. Chennaoui, M. Mountadar, M. Mohamme, M. Rihani, and O. Assobhei. 2013. The Physicochemical and Bacteriological Quality and Environmental Risks of Raw Sewage Rejected in the Coast of the City of El Jadida (Morocco). *Carpathian Journal of Earth and Environmental Sciences*. 8: 39–48.

[35] Hayatsu, M., C. Katsuyama, and K. Tago. 2021. Overview of Recent Researches on Nitrifying Microorganisms in Soil. *Soil Science and Plant Nutrition*. 67: 619–632. https://doi.org/10.1080/00380768.2021.1981119.

[36] Lehtovirta-Morley, L. E. 2018. Ammonia Oxidation: Ecology, Physiology, Biochemistry and Why They Must All Come Together. *FEMS Microbiology Letters*. 365(9). https://doi.org/10.1093/femsle/fny058.

[37] Chai, X., G. Li, Z. Chen, Z. Zhang, and R. Chi. 2020. Leaching Kinetics of Weathered Crust Elution-Deposited Rare Earth Ore with Compound Ammonium Carboxylate. *Frontiers in Chemistry*. https://doi.org/10.3389/fchem.2020.598752.

[38] Middleton, A., D. M. Park, Y. Jiao, and H. Hsu-Kim. 2020. Major Element Composition Controls Rare Earth Element Solubility during Leaching of Coal Fly Ash and Coal By-Products. *International Journal of Coal Geology*. 227: 103532. https://doi.org/10.1016/j.coal.2020.103532.

[39] Bhatt, V. 2016. Chapter 1 - Basic Coordination Chemistry. In *Academic Press*. 1–35. https://doi.org/10.1016/B978-0-12-803895-6.00001-X.

[40] Salazar-Salinas, K., P. A. Baldera-Aguayo, J. J. Encomendero-Risco, M. Orihuela, P. Sheen, J. M. Seminario, and M. Zimic. 2014. Metal-Ion Effects on the Polarization of Metal-Bound Water and Infrared Vibrational Modes of the Coordinated Metal Center of Mycobacterium Tuberculosis Pyrazinamidase via Quantum Mechanical Calculations. *Journal of Physical Chemistry B*. 118: 10065–10075. https://doi.org/10.1021/jp504096d.

[41] Haas, K. L., and K. J. Franz. 2009. Application of Metal Coordination Chemistry to Explore and Manipulate Cell Biology. *Chemical Reviews*. 109: 4921–4960. https://doi.org/10.1021/cr900134a.

[42] Yanfei, X., Zongyu, F., Xiaowei, H., Li, H., Yingying, C., Liangshi, W., and Zhiqi, L. 2015. Recovery of Rare Earths from Weathered Crust Elution-Deposited Rare Earth Ore without Ammonia-Nitrogen Pollution: I. Leaching with Magnesium Sulfate. *Hydrometallurgy*. 153: 58–65. https://doi.org/10.1016/j.hydromet.2015.02.011.

[43] Suraniti, E., P. Merzeau, J. Roche, S. Gounel, A. G. Mark, P. Fischer, N. Mano, and A. Kuhn. 2018. Uphill Production of Dihydrogen by Enzymatic Oxidation of Glucose without an External Energy Source. *Nature Communications* 9: 3229. https://doi.org/10.1038/s41467-018-05704-5.